LARGE DISPLACEMENT AND STABILITY ANALYSIS OF PLANE FRAMES USING ORAN'S TANGENT STIFFNESS MATRIX

Jarmo Salonen

Rakenteiden mekaniikka Vol. 22
No 2 1989, s. 3-22

Abstract: The beam-element of ORAN is presented in the article. The formulation uses ordinary dimensional forces and displacements in contrast to the original dimensionless formulation. The flexural bowing effect is taken into account quite accurately even in the presence of moderate member end rotations. Also the stability effects due to the axial force are taken into account. This formulation, which is based on the assumption of the Euler-Bernoulli hypothesis, seems to be the most accurate existing formulation for the large deflection analysis of elastic plane frames. Nevertheless, it is rather unknown to most people doing research in the areas relating to this subject. Numerical results of various nonlinear problems are given.

INTRODUCTION

The analysis is based on the Euler-Bernoulli beam theory. Accordingly the shear deflections are neglected and plane cross-sections will remain plane and perpendicular to the centre-line after deformations. The bending moment is directly proportional to the curvature of the beam's centre-line. The technique for solving the governing differential equations for some frame structures is called elastica analysis. Usually the axial deformations caused by normal forces are neglected, but recently [8] they have been taken into consideration.

Various numerical formulations for the analysis of geometrically nonlinear framed structures, using the finite element displacement method, have been presented in the literature. Many formulations are based on nonlinear strain and stress quantities. Numerical integration is necessary for computing the element stiffness matrices and nodal force vectors. The alternative approach is called the beam-column formulation. ORAN's formulation uses explicit stiffness matrices and nodal force vectors, which is typical of the latter approach. Rather than give references to various

formulations, the writer will describe ORAN's formulation and references are given only to the other related beam-column formulations.

The differential equation relating bending moment to curvature is linearized and using some additional assumptions one arrives at the well-known relationship connecting the element's end-rotations and end-moments. The stability functions in this relationship are functions of the element's axial force. The relationship used for calculating the axial force under the flexural deformations has been given by SAAFAN [10] and is somewhat less well-known. The bowing functions in this relationship are also functions of the axial force itself.

An element's end-rotations and the change in its chord length are the basic deformations used in the relationships for determining the basic forces of the element. They can be easily calculated from the element's nodal displacements. The element's nodal forces are then determined in the global coordinate-system directions. The assembled nodal force vector from all the elements must then balance the external loading which is thought to be concentrated on the structure's nodes. The problem of the large displacement analysis is to find the deformed configuration of the structure that will satisfy the system's force equilibrium equations. The accuracy of the formulation depends solely on the element's basic force-deformation relationships that were mentioned.

Solution techniques for finding the equilibrium satisfying displacement configuration are, among others, the secant stiffness iteration and the more commonly used incremental Newton-Raphson iteration. The latter uses the system's tangent stiffness matrix which is assembled from the element tangent stiffness matrices. The basic force-deformation relationship used here is very nonlinear and in order to achieve convergence rapidly during the iteration process one must use accurate tangent stiffness matrices. The tangent stiffness matrix of ORAN [1] is consistent (exact) with the basic force-deformation relationship and thus it provides optimum convergence properties. The simplified tangent stiffness matrix has been given by VIRTANEN & MIKKOLA [12]. The authors used the arc length method with the modified Newton-Raphson iteration. ORAN's stiffness matrix was also used for the numerical results, and the effect of bowing was examined. LUI & CHEN [7] used the same simplified stiffness matrix in their study of frames with nonlinear flexible joints.

The original formulation of ORAN is rewritten by the author in order to utilize ordinary dimensional forces and displacements. Some different sign conventions are also used. The computer program has been made by the writer. It is capable of analysing elastic-plastic plane frames and truss elements can also be included in the structures. The theory's extension has been given by KASSIMALI [2] and is not included in this article.

THE BASIC FORCE-DEFORMATION RELATIONSHIP

The linearized differential equation resulting from the Euler-Bernoulli beam theory is

$$EIv''(x) - Pv = -M_A + \frac{M_A + M_B}{L} x \quad . \tag{1}$$

The curvature has been approximated by the second derivative of the deflection v(x) and the element's chord length is taken to be the original length of the element. The deflection v(x) is determined and, further, using approximations for the element's end-rotations, namely $\theta_A = v'(0)$ and $\theta_B = v'(L)$, the relation between end-moments and end-rotations is

$$\begin{bmatrix} M_A \\ M_B \end{bmatrix} = \frac{EI}{L} \begin{bmatrix} c_1 & c_2 \\ c_2 & c_1 \end{bmatrix} \begin{bmatrix} \theta_A \\ \theta_B \end{bmatrix} \quad . \tag{2}$$

The stability functions c_i in (2) are

$$c_1 = \frac{\phi\ (\sin\phi - \phi\cos\phi)}{2(1 - \cos\phi) - \phi\sin\phi} \quad , \tag{3}$$

$$c_2 = \frac{\phi\ (\phi - \sin\phi)}{2(1 - \cos\phi) - \phi\sin\phi} \quad , \tag{4}$$

when $\rho < 0$ (compressive axial force) and

$$c_1 = \frac{\phi\ (\phi\cosh\phi - \sinh\phi)}{2(1 - \cosh\phi) + \phi\sinh\phi} \quad , \tag{5}$$

$$c_2 = \frac{\phi(\sinh\phi - \phi)}{2(1 - \cosh\phi) + \phi\sinh\phi} \quad , \tag{6}$$

when $\rho > 0$ (tensile axial force) .

The parameter ρ is the dimensionless axial force defined by

$$\rho = \frac{P\,L^2}{\pi^2\,EI} \quad . \tag{7}$$

The argument of the stability functions is

$$\phi = \pi \sqrt{|\rho|} \quad . \tag{8}$$

The element's moment-rotation relationship was determined using the original length of the element. Accordingly the arc length of the element is given by the integral

$$s = L + e_c = \int_0^L (1 + (v')^2)^{1/2}\,dx \quad . \tag{9}$$

The term e_c represents the length correction due to the bowing effect.

$$e_c \approx \int_0^L \frac{1}{2}\,(v')^2\,dx \quad . \tag{10}$$

The axial force of the element is

$$P = \frac{EA}{L}\,(e + e_c) \quad , \tag{11}$$

where e is the change in the chord length of the element defined by $L_\ell = L + e$. L_ℓ is the element's chord length in the deformed state.

SAAFAN [10] has given the formula for the bowing term

$$e_c = [b_1(\theta_A + \theta_B)^2 + b_2(\theta_A - \theta_B)^2]\,L \quad . \tag{12}$$

It is deducible from the Eq. (10). The bowing b_i functions in Eq. (12) are therefore functions of the stability functions and are given by

$$b_1 = \frac{-(c_1 + c_2)\,(c_2 - 2)}{8\,\pi^2\,\rho} \quad , \tag{13}$$

$$b_2 = \frac{c_2}{8(c_1 + c_2)} \quad . \tag{14}$$

When the axial force $\rho = 0$, the denominators of the expressions for the stability functions and also that of the bowing function b_1 are zero and computational difficulties are encountered in the evaluation of these functions using given formulas. The series expressions are to be used when $|\rho| < 0.1$. They were given by KASSIMALI [2] and are also to be found in [3] and in Appendix A.

THE INCREMENTAL BASIC FORCE-DEFORMATION RELATIONSHIP

The basic element force and the corresponding deformation vectors are

$$r_c = \{ M_A \; M_B \; P \} \quad , \tag{15}$$

$$d_c = \{ \theta_A \; \theta_B \; e \} \quad . \tag{16}$$

The incremental force-deformation relationship is expressed as

$$\dot{r}_c = \dot{k}_c \; \dot{d}_c \quad . \tag{17}$$

The basic incremental stiffness matrix $\dot{k}_c$ in the relation (17) is obtained by differentiating the relations $r_{ci} = r_{ci}(d_{cj} \; , \; \rho(d_{cj}))$ that were given by relationship (2) and Eq. (11) . The vectors and the matrix in (17) are

$$\dot{d}_c = \{ d\theta_A \quad d\theta_B \quad de \} = \{ \dot{\theta}_A \quad \dot{\theta}_B \quad \dot{e} \} \quad , \tag{18}$$

$$\dot{r}_c = \{ dM_A \quad dM_B \quad dP \} = \{ \dot{M}_A \quad \dot{M}_B \quad \dot{P} \} \quad . \tag{19}$$

$$\dot{k}_{cij} = \frac{\partial r_{ci}}{\partial d_{cj}} + \frac{\partial r_{ci}}{\partial \rho} \; \frac{\partial \rho}{\partial d_{cj}} \quad . \tag{20}$$

The basic incremental stiffness matrix was given by ORAN [1]. It is

$$\dot{k}_c = \frac{EI}{L} \begin{bmatrix} c_1 + \frac{G_1^2}{H} & c_2 + \frac{G_1 G_2}{H} & \frac{G_1}{HL} \\ & c_1 + \frac{G_2^2}{H} & \frac{G_2}{HL} \\ S \; Y \; M. & & \frac{1}{HL^2} \end{bmatrix} \quad . \tag{21}$$

The G_1 and H functions are

$$G_1 = 2 \; [(b_1 + b_2)\theta_A + (b_1 - b_2)\theta_B] \quad , \tag{22}$$

$$G_2 = 2 \; [(b_1 - b_2)\theta_A + (b_1 + b_2)\theta_B] \quad , \tag{23}$$

$$H = \frac{I}{AL^2} - \frac{1}{\pi^2}\left[b_1'(\theta_A + \theta_B)^2 + b_2'(\theta_A - \theta_B)^2\right] \quad . \tag{24}$$

The last one uses derivatives of the bowing functions with respect to the dimensionless axial force of the element. They are

$$b_1' = -\frac{(b_1 - b_2)(c_1 + c_2) + 2c_2b_1}{4\rho} \quad , \tag{25}$$

$$b_2' = -\frac{\pi^2(16b_1b_2 - b_1 + b_2)}{4(c_1 + c_2)} \quad . \tag{26}$$

Here again the series expression is to be used for b_1' when $|\rho| < 0.1$. It was given in [2] and can also be found in Appendix A. It should be pointed out that KASSIMALI [2] used ORAN's sign convention for the axial force. The dimensionless axial force was $q = -\rho$ and the derivatives in his article were taken with respect to this parameter. In articles [12] & [7] the G_1^2/H , G_1G_2/H and the second term in H were neglected in the $\dot{k}_c$ matrix. Numerical difficulties have been experienced using this simplified matrix. Many elements have to be used for one natural element, particularly with quite slender beams, in order to avoid convergence difficulties with the Newton-Raphson iteration.

THE INCREMENTAL FORCE-DISPLACEMENT RELATIONSHIP

The element's deformations are related to its displacements by the kinematic equations

$$d_{c1} = d_{g3} - (\theta - \theta_0) \quad , \tag{27}$$

$$d_{c2} = d_{g6} - (\theta - \theta_0) \quad , \tag{28}$$

$$d_{c3} = L_f - L \quad . \tag{29}$$

The θ is the angle of the element's chord in the deformed configuration, and L_f is the chord length. They are expressed in terms of the element's displacements by the equations

$$\theta = \arctan\left(\frac{y_0 + d_{g5} - d_{g2}}{x_0 + d_{g4} - d_{g1}}\right) \quad \text{and} \tag{30}$$

$$L_f = \left[(x_0 + d_{g4} - d_{g1})^2 + (y_0 + d_{g5} - d_{g2})^2\right]^{1/2} \quad . \tag{31}$$

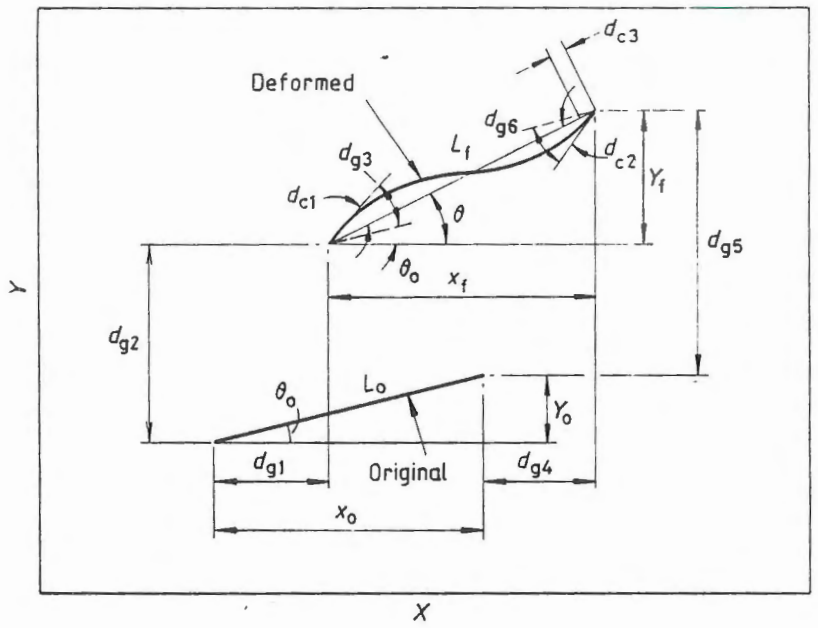

Figure 1. Kinematic relationship between deformations and displacements

The increments of the deformations are related to the increments of the displacements by the transformation

$$\dot{d}_c = T_{cg}\dot{d}_g \quad . \tag{32}$$

The components of the transformation matrix T_{cg} are

$$T_{cgij} = \frac{\partial d_{ci}}{\partial d_{gj}} \quad . \tag{33}$$

The transformation matrix is

$$T_{cg} = \begin{bmatrix} -s/L_f & c/L_f & 1 & s/L_f & -c/L_f & 0 \\ -s/L_f & c/L_f & 0 & s/L_f & -c/L_f & 1 \\ -c & -s & 0 & c & s & 0 \end{bmatrix} \quad , \tag{34}$$

where $c = \cos\theta$ and $s = \sin\theta$.

The element's nodal forces are related to its basic forces by the transformation

$$r_g = T_{cg}^T r_c \quad . \tag{35}$$

The components of the element's tangent stiffness matrix are given by

$$\dot{k}_{gij} = \frac{\partial \dot{r}_{gi}}{\partial d_{gj}} \quad , \; i,j = 1..6 \tag{36}$$

By the differentiation of the Eqs (35), using the relations (17) and (32), one can develop the following relation between the increments of the element's nodal forces and displacements

$$\dot{r}_{gi} = T_{cgji}\dot{k}_{cjk}T_{cgkl}\,\dot{d}_{gl} + \left(\frac{\partial^2 d_{c1}}{\partial d_{gi}\partial d_{gk}}\, r_{c1} + \frac{\partial^2 d_{c2}}{\partial d_{gi}\partial d_{gk}}\, r_{c2} + \frac{\partial^2 d_{c3}}{\partial d_{gi}\partial d_{gk}}\, r_{c3} \right) \dot{d}_{gk} \quad . \tag{37}$$

The repeating subscripts in Eq. (37) are summation indices and the subscripts c and g should not be mixed with vector or matrix component indices.

The incremental force-displacement relationship is given in matrix notation

$$\dot{r}_g = \left[T_{cg}^T \dot{k}_c T_{cg} + \sum_1^3 T_i\, r_{ci} \right] \dot{d}_g \quad . \tag{38}$$

The tangent stiffness matrix $\dot{k}_g$ defined by (38) is exact, meaning that it is derived from the basic element force-deformation relationship without any further simplifications.

The T_i -matrices are

$$T_1 = T_2 = \frac{1}{L_f^2}\begin{bmatrix} -2cs & c^2-s^2 & 0 & 2cs & -(c^2-s^2) & 0 \\ & 2cs & 0 & -(c^2-s^2) & -2cs & 0 \\ & & 0 & 0 & 0 & 0 \\ & & & -2cs & c^2-s^2 & 0 \\ & & & & 2cs & 0 \\ & \text{SYM} & & & & 0 \end{bmatrix} , \tag{39}$$

$$T_3 = \frac{1}{L_f}\begin{bmatrix} s^2 & -cs & 0 & -s^2 & cs & 0 \\ & c^2 & 0 & cs & -c^2 & 0 \\ & & 0 & 0 & 0 & 0 \\ & & & s^2 & -cs & 0 \\ & & & & c^2 & 0 \\ & \text{SYM} & & & & 0 \end{bmatrix} . \tag{40}$$

EQUILIBRIUM ITERATION

The displacement vector D_g, containing the structure's cumulative degrees of freedom is updated with the incremental displacement vector $\dot{D}_g$. The update is obtained from the Newton-Raphson iteration which uses the difference of the external loading vector and the nodal force vector R_g as the unbalanced force vector. The nodal force vector is assembled from the nodal force vectors of the elements. The r_g vectors are calculated from the current nodal displacements. From Eqs. (27)..(29) => d_c , (2)&(11) => r_c , (35) => r_g . The Newton-Raphson iteration algorithm is described in Appendix B.

The computation of the axial force P from the Eq. (11) has to be done iteratively for every element. Equation (11) can be rewritten as

$$K(\rho) = \frac{\pi^2 I}{AL^2}\rho - \left(\frac{e}{L} + \frac{e_c(\rho)}{L}\right) = 0 \quad . \tag{41}$$

The iteration formula for the dimensionless axial force is

$$\rho_{i+1} = \rho_i - \frac{K(\rho_i)}{K'(\rho_i)} \quad , \tag{42}$$

where the derivative of the nonlinear function is

$$K'(\rho) = \frac{\pi^2 I}{AL^2} - [b_1'(\theta_A + \theta_B)^2 + b_2'(\theta_A - \theta_B)^2] \quad . \tag{43}$$

The initial value is usually quite accurately known and the iteration will converge very rapidly.

The convergence rate of the global Newton-Raphson iteration is dependent on the size of the loading increments and it is usually also good. For very slender structures the loading increments have to be kept small because of the strong influence of the axial force on the flexural stiffness. It is recommended that the slenderness ratio

$$\lambda = L\sqrt{A/I} \quad , \tag{44}$$

where L is some typical length of the structure, have a value less than 1000 . Experience has shown also that the modified Newton-Raphson iteration technique, in which the structure's tangent stiffness matrix is updated only at the first iteration of every load step, is to be avoided. Due to

the very nonlinear nature of the formulation, the resulting updated configurations will have quite different associated tangent stiffness matrices for the structure, and the accurately computed unbalanced force vectors will bounce the structure from one erroneous configuration to another.

An automated path-following technique for passing the snap-through limit points and tracing the structure's behaviour into the post-critical range is required. The arc length procedure used in the numerical example of the stability analysis for calculating the structure's limit point accurately is described in [6] by FORDE & STIEMER.

NUMERICAL EXAMPLES

The computation has been done with a computer program which uses double precision variables. The program has been compiled by the DEC-Pascal compiler. It has the capability of analysing also elastic-plastic frames with the concept of introducing plastic hinges to the ends of the elements during the course of the analysis. It is based on KASSIMALI's article [2], and has been documented also in [4].

Large displacement analyses

Example 1.
The cantilever beam with concentrated transverse load at its end

This is perhaps the most commonly used test problem for various large deflection beam element formulations. The numerical results of the elastica analysis have been given in [5] by MATTIASSON. The axial deformation caused by normal force is neglected in these results. Accordingly the slenderness ratio must be chosen sufficiently large. With the values $L = 1000$, $I = 1$ and $A = 1$, $\lambda = 1000$. The results at the load level $PL^2/EI = 10$ are

$$w/L = 0.81061 \ , \quad u/L = 0.55500 \ , \quad \theta_0 = 1.43029 \text{ rad} \ . \qquad (45)$$

The same problem has also been analyzed by HOLOPAINEN in [11] using the force method.

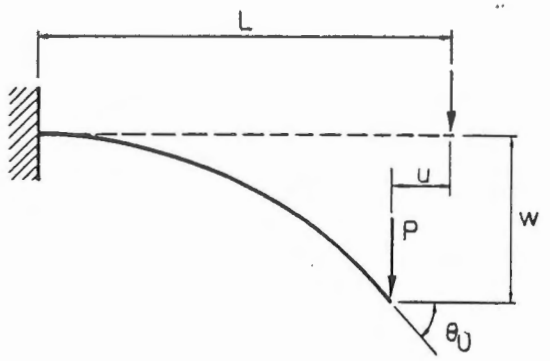

Figure 2. Cantilever with transverse point load at the free end

Table 1. Deflections at the free end for the cantilever beam in Fig. 2 , $PL^2/EI = 10$, $L = 1000$, $\lambda = 1000$

Elements	w	u	θ_0
1	800.57	537.34	1.41484
2	807.31	551.52	1.42879
3	809.60	554.16	1.42994
4	810.25	554.73	1.43017
8	810.59	554.98	1.43028
16	810.62	554.99	1.43029

The load increments at the beginning of the analysis have to be small because $\lambda = 1000$. The increment $\Delta P_0 = 0.2$ was used. The displaced configuration at the final load level $P = 10$ is such that the beam is loaded also with quite substantial axial force, and for lower slenderness ratios also some axial deformation would occur. The deformed configuration is shown in Fig. 3. In computing Table 1, the cantilever was divided into elements of equal length. Better results could be obtained with fewer elements using denser discretization at the supported end of the structure.

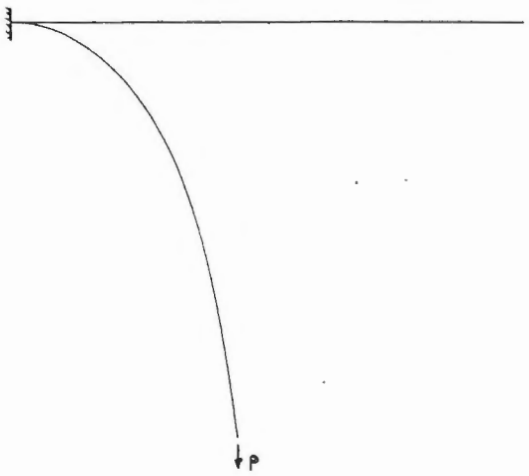

Figure 3. The deformed shape of the cantilever , $PL^2/EI = 10$

Example 2.
The cantilever beam with moment load at its free end

This loading deforms the cantilever into a circular arc. At the value of $M = 2\pi EI/L$ the cantilever is bent into a closed circle of diameter $D = L/\pi$, L being the length of the cantilever. The structure is divided into four equal elements and the loading is increased gradually during the analysis to $M = 2\pi EI/L$. From Fig. 4 it can be observed that the end-rotations of each element are 45 degrees.

The numerical values used for the analysis are $L = 100$, $I = 1$, $A = 1$, $E = 1$. The slenderness ratio $\lambda = 100$.

The free end node 5 is almost exactly coincident with the fixed end node 1. This result has been obtained also with the more simple ANSYS STIF3 elements [9]. The intermediate nodes 2,3 and 4 are very accurately on the circle whose diameter is $D = 31.7205$. The exact theoretical value is $D_{exact} \approx 31.83099$. The relative error is -0.35% . The loading was applied in ten equal increments and the number of iterations was 8 for every load step.

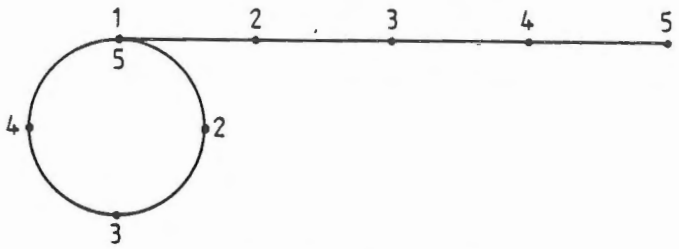

Figure 4. The deformed shape of the cantilever , M = $2\pi EI/L$

Despite the quite normal slenderness ratio, this problem demanded surprisingly small load increments and also many (8) iterations in each load step. This property may be due to the absence of the axial force. Some beam element formulations allow the application of larger load increments, but they are also always less accurate. This is the price that has to be paid for accuracy.

The same model was also analyzed with the 8-element model and the relative error in the diameter of the circle was then only -0.02% . Increasing the load to M = $2*2\pi EI/L$ deforms the structure into a circle with the diameter $D_{exact} = L/(2\pi)$. The relative error in the computed value is now the same as before, namely -0.35% . The coincident nodes in this nine node model are (1,5,9), (2,6), (3,7), (4,8). The accuracy of the formulation is much better than is to be expected from the approximations that were made in the development of the basic force-deformation relationship. This example demonstrates also that the formulation does not require any restrictions on the rigid-body rotations of each element. This should be obvious from the theory.

Example 3.
The square frame loaded at the midpoints of opposite sides

The structure is pictured in Fig. 5. The displacement components in it have been tabulated in [5] by MATTIASSON as functions of the loading parameter PL^2/EI. These results are from the elastica analysis, neglecting the influence of the axial force on the deformations. The loading is primarily of the bending type and λ does not need to be very large in order to get comparable results with the program.

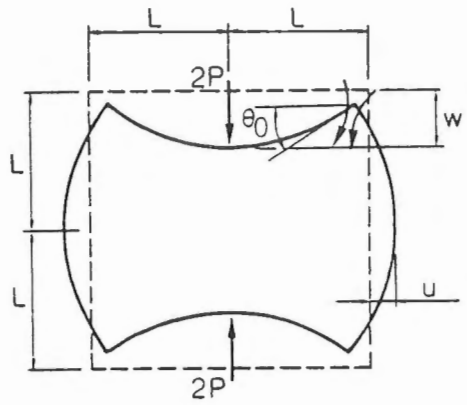

Figure 5. Square frame loaded in compression

The chosen values are L = 1000 mm, I = 4.761905 mm^4, A = 1 mm^2 and E = $210*10^3 N/mm^2$. The slenderness ratio is $L\sqrt{A/I} \approx 458$.

The largest loading value in [5] is $PL^2/EI = 4$, and the corresponding elastica results are compared with the formulation used here. The elastica results are

$$w/L = 1.17703 \qquad u/L = 0.33754 \quad . \tag{46}$$

The computed values are given in Table 2 along with the results obtained with the general purpose FEM-code ANSYS using ordinary small-deformation large-deflection STIF3 elements. The symbol e in the table is the number of elements used in the model for one natural element. The final load could be applied by incrementing the loading in four equal increments, although better convergence would be obtained using smaller load increments.

Table 2. Deflections w and u for the square frame, $PL^2/EI = 4.0$, L = 1000 , $\lambda \approx 458$

e	w, ORAN	w, ANSYS	u, ORAN	u, ANSYS
1	1139.42	1261.62	334.065	446.478
2	1175.30	1160.58	337.510	356.305
3	1176.70	1167.54	337.582	345.867
4	1176.93	1171.26	337.553	342.280
8	1177.04	-------	337.539	-------

The computational model that was used utilized the frame's double symmetry. The displaced configuration is shown in Fig. 6.

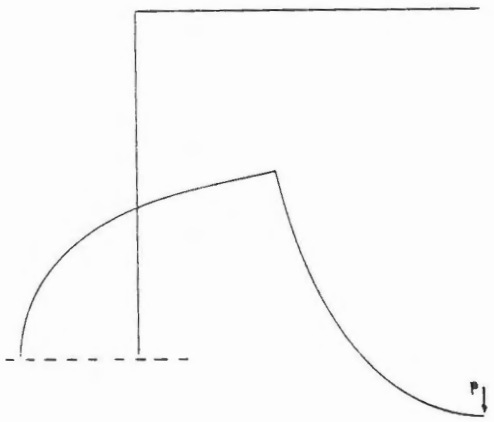

Figure 6. The deformed shape of the square frame , $PL^2/EI = 4.0$

Stability analysis

In the foregoing numerical examples the displacements have been fairly large. One very important feature of the nonlinear formulation is its ability to handle small deflection stability analysis problems with very few elements. ORAN's formulation makes it possible to use only one element for each natural element in a structure.

Example 4.
Two-bar frame, stability problem

KOUNADIS [8] has analysed the frame in this example using exact elastica analysis. The analysis also takes the axial deformations into account. The critical loading in this structure is associated with a limit point instability phenomenon. According to the standard elastica analysis, neglecting the axial deformations, failure will occur with the bifurcation of the structure. The structure's geometry is shown in Fig. 7. The numerical values are: L = 100, I = 1, A = 0.16 => $\lambda = 40$, E = 100. The critical load and the corresponding horizontal displacement of the corner are according to exact elastica analysis

$$\frac{PL^2}{EI} = 1.32617 \ , \qquad u \approx 2.3 \ , \tag{47}$$

the displacement being to the left. The bifurcation load from the standard elastica solution is 1.42196 , with no horizontal displacements prior to buckling.

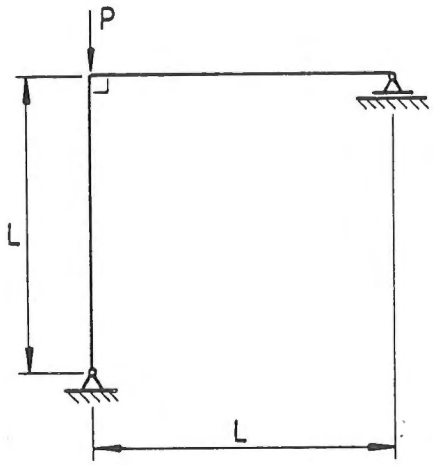

Figure 7. Geometry and loading of the two-bar frame

The determination of the ultimate critical load is impossible with the standard load incrementing N-R iteration if it is desired to compute with as high accuracy as in the above results. The so-called arc length method procedure is used. The load-displacement path is followed automatically during the analysis procedure.

The nature of the failure can be seen from Fig. 8. The corner node's horizontal displacement is monitored in the vicinity of the critical loading. The model from which these results were calculated used 8 elements of equal length. The numerical results for the critical load and the associated displacement are given in Table 3.

The values in Table 3 were computed using quite small arc-lengths. Using even smaller arc-lengths they might change a little. Especially the displacement u varies very much for even slight changes in the load factor. This can be seen from Fig. 8. The critical load from the eight element model is the same as from the exact analysis. The small difference in the two element model is probably due to the axial deformations.

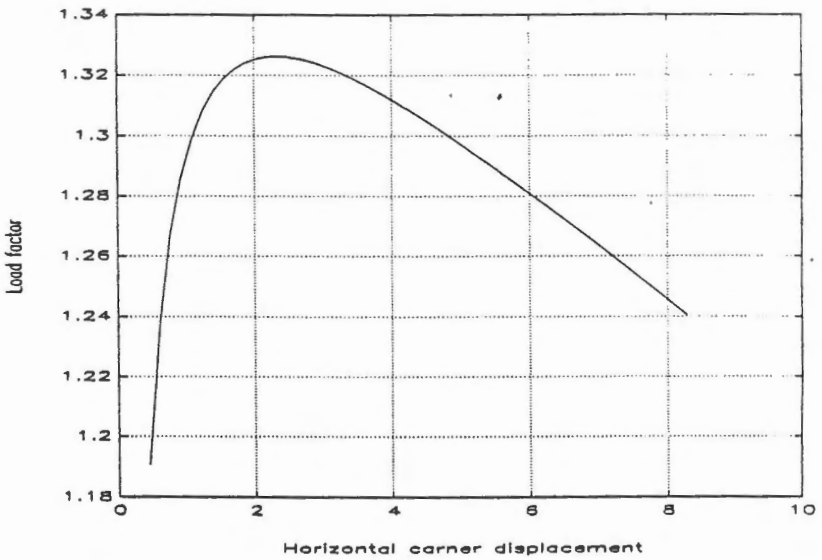

Figure 8. Loading $PL^2/(EI)$ vs horizontal displacement u , L = 100

Table 3. Critical load and displacement u for the two-bar frame by ORAN's formulation, L = 100, λ = 40

Elements	PL^2/EI	u
2	1.326118	2.30
4	1.326158	2.31
6	1.326166	2.30
8	1.326169	2.30

CONCLUSIONS

The accuracy of the presented beam element formulation was examined using three large deflection problems and one stability analysis problem. The results were compared with exact solutions found in the literature. Non-linear analyses can be done with the element models using very few elements and therefore with only few degrees of freedom. The formulation is very accurate and also practical to use in analysing frame structures. The tangent stiffness matrix is easy to modify for hinged connections and the modified formulation can then be applied for structures consisting of beam or truss elements, or combinations of them.

REFERENCES

1. Oran,C., Tangent Stiffness in Plane Frames, Journal of the Structural Division, Vol 99, No. ST6, June ,1973, pp. 973..985.

2. Kassimali,A., Large Deformation Analysis of Elastic-Plastic Frames, Journal of Structural Engineering, Vol 109, No. 8, August, 1983, pp. 1869..1886.

3. Salonen,J., Yhteenveto ORANin epälineaarisesta tasopalkkielementistä, Tampere University of Technology, Dept. of Mech. Eng., Applied Mech., Research Raport 49, 1989, p. 64.

4. Salonen,J., Holopainen,P., Kimmoplastisten tasokehien laskenta ottaen huomioon suuret siirtymät, Tampere University of Technology, Dept. of Mech. Eng., Applied Mechanics, Research Raport 44, 1988, p. 106.

5. Mattiasson,K., Numerical Results from Large Deflection Beam and Frame Problems Analysed by Means of Elliptic Integrals, International Journal for Numerical Methods in Engineering, Vol 17., No. 1, 1981, pp. 145..153.

6. Forde,B., Stiemer,S., Improved Arc Length Orthogonality Methods for Nonlinear Finite Element Analysis, Computers & Structures, Vol. 27, No. 5., 1987, pp. 625..630.

7. Lui,E,M.,Chen,W.F, Analysis and Behaviour of Flexibly-jointed Frames, Engineering Structures, Vol 8., Number 2, April, 1986, pp. 107..118.

8. Kounadis,A.N, Efficiency and Accuracy of Linearized Postbuckling Analyses of Frames based on Elastica, Int. J. Solids Structures, Vol 24, No. 11, 1988, pp. 1097..1112.

9. Kohnke,P., Large Deflection Analysis of Frame Structures by Fictitious Forces, International Journal for Numerical Methods in Engineering, Vol 12, No. 8, 1978, pp. 1279..1294.

10. Saafan,S., Nonlinear behaviour of Structural Plane Frames, Journal of the Structural division, ASCE, Vol 89, No. ST4, Proc Paper 3615, August, 1963, pp. 557..579.

11. Holopainen,P., The General Theory of a Suspension Cable, Doctoral Dissertation, Helsinki University of Technology, 1975, p. 65.

12. Virtanen,H., Mikkola,M., Tasokehien geometrisesti epälineaarinen analysointi, Rakenteiden Mekaniikka, Vol. 18, No 1, 1985, pp. 53..68.

APPENDIX A

The series expressions [2] of the stability functions are

$$c_1 \approx 4 + \frac{2}{15}\pi^2\rho - \frac{11}{6300}\pi^4\rho^2 + \frac{1}{27000}\pi^6\rho^3 \quad , \tag{A1}$$

$$c_2 \approx 2 - \frac{1}{30}\pi^2\rho + \frac{13}{12600}\pi^4\rho^2 - \frac{11}{378000}\pi^6\rho^3 \quad . \tag{A2}$$

The series expressions of the bowing function b_1 and its derivative b_1' are

$$b_1 \approx \frac{1}{40} - \frac{1}{2800}\pi^2\rho + \frac{1}{168000}\pi^4\rho^2 - \frac{37}{388080000}\pi^6\rho^3 \quad , \tag{A3}$$

$$b_1' \approx -\frac{1}{2800}\pi^2 + \frac{1}{84000}\pi^4\rho - \frac{37}{129360000}\pi^6\rho^2 \quad . \tag{A4}$$

APPENDIX B

The algorithm below is given to clarify the Newton-Raphson iteration and the incremental load-increasing procedure.

```
REPEAT
|   P_g = P_g + ΔP_g                 - increase applied load vector
|   i = 0   ,  R_g^0 is the nodal force vector of the previous
|               converged load step.
|   REPEAT                           - NR-iteration loop
|   |
|   |   K_g^i = Σ_1^e A^s k_g^i      - assembly procedure
|   |
|   |   P_g - R_g^i = K_g^i ΔD_g^(i+1)   - solution => ΔD_g^(i+1)
|   |
|   |   D_g^(i+1) = D_g^i + ΔD_g^(i+1)   - update displacement configuration
|   |
|   |   IF converged(D_g^(i+1) , ΔD_g^(i+1)) THEN next_loadstep = TRUE
|   |
|   |   R_g^(i+1) = Σ_1^e A^s r_g^(i+1)  - nodal force vector
|   |
|   |          ( D_g^(i+1) => d_g => d_c => r_c => r_g^(i+1) )
|   |   IF wanted print_results
|   |   i = i + 1
|   UNTIL next_loadstep
UNTIL end_of_analysis
```

The arc length method is based on the idea of tracing the load-displacement response in the load-displacement space by the constant arc length steps. In the NR-loop the applied loading is changed by the restriction algorithm. The details can be found in [6]. The convergence characteristics are better than in the pure NR-iteration and convergence should be obtained also with the modified Newton-Raphson iteration. The drawback is for the user to not be able to control the applied loading anymore. This is done automatically by the constant arc length restriction.

Jarmo Salonen, dipl.ins., Tampereen teknillinen korkeakoulu,
Konetekniikan osasto, Teknillisen mekaniikan laitos